OPEN ACCESS
IOP Publishing
Journal of Optics
J. Opt. **23** (2021) 015003 (9pp)
https://doi.org/10.1088/2040-8986/abcfd6

Long-distance heat transfer between molecular systems through a hybrid plasmonic-photonic nanoresonator

S Mahmoud Ashrafi[1], R Malekfar[1], A R Bahrampour[2] and Johannes Feist[3]

[1] Department of Physics, Tarbiat Modares University, Tehran, Iran
[2] Department of Physics, Sharif University of Technology, Tehran, Iran
[3] Departamento de Física Teórica de la Materia Condensada and Condensed Matter Physics Center (IFIMAC), Universidad Autónoma de Madrid, E-28049 Madrid, Spain

E-mail: johannes.feist@uam.es

Received 25 August 2020, revised 10 November 2020
Accepted for publication 2 December 2020
Published 24 December 2020

Abstract

We theoretically study a hybrid plasmonic-photonic cavity setup that can be used to induce and control long-distance heat transfer between molecular systems through optomechanical interactions. The structure we propose consists of two separated plasmonic nanoantennas coupled to a dielectric cavity. The hybrid modes of this resonator can combine the large optomechanical coupling of the sub-wavelength plasmonic modes with the large quality factor and delocalized character of the cavity mode that extends over a large distance ($\sim\mu$m). We show that this can lead to effective long-range heat transport between molecular vibrations that can be actively controlled through an external driving laser.

Keywords: optomechanics, heat transfer, molecular optomechanics, hybrid plasmonic-photonic

(Some figures may appear in colour only in the online journal)

1. Introduction

Energy transfer between quantum emitters (quantum dots, molecules, atoms, …) is a process of fundamental importance for a large range of phenomena in quantum information, quantum thermodynamics, quantum biology, photosynthesis, solar cells, etc [1–9]. One powerful strategy to modify these processes is by coupling the emitters with an electromagnetic mode and mediating transport through photon absorption and emission [10–13]. Since the light-matter coupling strength is inversely proportional to the effective mode volume, the largest single-emitter coupling strengths up to now have been reached with nanoplasmonic resonators due to their ability to confine light in ultra-small sub-wavelength volumes down to $V_p \approx 10^{-8}\lambda^3$ [14–16], where λ is the free-space wavelength. These capabilities have led to a large range of applications of nanoplasmonic systems [17], including in the context of quantum electrodynamics (QED) and quantum optics, such as for strong coupling with a single molecule at room temperature [15, 16] or single-photon sources [18, 19].

Over the last few years, it has also been realized that the process of surface-enhanced Raman scattering, which is a well-known strategy for enhancing the Raman scattering signal of molecules by many orders of magnitude [20, 21], can alternatively be interpreted through the framework of quantum optomechanics [22, 23]. In this context, we have recently shown that a localized surface plasmon resonance (LSPR) modes can mediate heat transfer between two molecules through its optomechanical coupling to the vibrations in each molecule [24]. However, this approach is limited in practice due to the required small (nm-scale) distance between molecules coupled to the same sub-wavelength LSPR

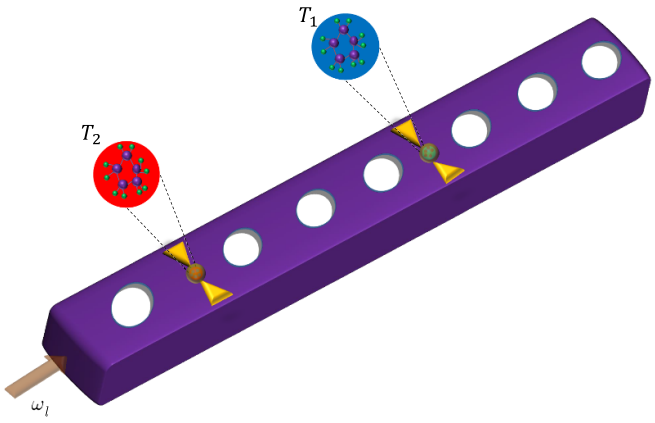

Figure 1. Sketch of the hybrid plasmonic-photonic nanoresonator containing two separated molecules placed in the hot spots of two bowtie nanoantennas with different temperatures (the red circle displays a 'hot' molecule and the blue circle displays a 'cold' molecule).

mode, and additionally suffers from the low quality factors ($Q \sim 10$) of plasmonic resonators that are unavoidable due to the large intrinsic losses of the metals providing the sub-wavelength confinement. Hybrid plasmonic-photonic (i.e. metallo-dielectric) cavities present an intriguing possibility to circumvent these limitations. In spite of the large size difference between plasmonic nanoparticles and dielectric cavities, their optical resonances can be tuned to comparable frequencies, leading to significant hybridization between these modes. The new hybrid modes can then combine the strong light-matter interactions of plasmonic systems with the possible large lifetimes (high quality factors) of dielectric structures. Such approaches have been shown to improve the performance of existing applications and allow novel applications for a broad range of examples such as strong light-matter coupling [25–27], optical trapping [28], surface-enhanced Raman scattering [29], label-free detection of molecules [30, 31], biosensing [32], optoplasmonic sensors [33], or refractometers and nanoparticle trapping [34].

In this article, we theoretically and numerically show that a hybrid photonic-plasmonic cavity can enable efficient long-range heat transfer between spatially separated molecules through optomechanical interactions. The setup we propose, sketched in figure 1, consists of two metallic nanoantennas coupled to a photonic cavity such as a photonic crystal (PC) beam or a dielectric mirror cavity. Such a system supports two different kinds of electromagnetic modes, strongly localized LSPR modes on each nanoantenna, and an extended cavity mode, which we assume to be driven by an external laser. The maximum distance between the nanoantennas is determined by the extension of the cavity mode and can be on the order of (several times) the laser wavelength. A molecule is placed in the hot spot of each nanoantenna, with each molecule coupled to a local heat bath at temperature T_1 (cold) and T_2 (hot), respectively. As we will show below, such a system can be used to efficiently transfer heat between the molecular vibrational modes, with the driving laser providing active control over the heat transfer process.

The paper is organized as follows: in section 2, we introduce the quantum optomechanical model we use, both in terms of the original uncoupled (LSPR and PC) modes as well as in terms of hybrid modes obtained from their coupling. In section 3, we present the main results, including a discussion of the influence of the main parameters of the system, and in particular show the consequence of coupling between vibrational modes of different frequencies. We conclude with a section summarizing and discussing the results.

2. Theoretical model and framework

Our model, schematically depicted in figure 2, treats three photonic modes and two molecules. We note that while the direct quantization of hybrid cavity modes is far from trivial [35, 36], we have recently shown that they can be represented accurately within a description containing a few interacting modes (without counterrotating terms) that each decay independently [37]. The model we use in the following is based on such a description. The three photonic modes are given by one cavity mode, with frequency ω_c and bosonic annihilation operator a_c, and two LSPRs, with frequencies $\omega_{p,i}$ and bosonic annihilation operators $a_{p,i}$ ($i = 1, 2$). One molecule is assumed to be placed in the hot spot of each LSPR, with each molecule represented by a single vibrational mode. These modes are approximated as harmonic oscillators, with frequencies ν_j and annihilation operators b_j ($j = 1, 2$). We assume that an external continuous-wave laser with frequency ω_l and amplitude Ω drives the cavity mode. The laser bandwidth is assumed to be small enough compared to the relevant system bandwidths that it can be represented as an idealized single-frequency light source. The total Hamiltonian of the system in the rotating frame of the laser and within the rotating wave approximation can then be written as (here and in the following, we set $\hbar = 1$)

$$H = H_{\rm ph} + H_{\rm m} + H_{\rm I} + H_{\rm d}, \tag{1a}$$

$$H_{\rm ph} = \sum_{\alpha} \delta_\alpha a_\alpha^\dagger a_\alpha + \sum_{i=1}^{2} g_{\rm cp}(a_c^\dagger a_{p,i} + a_c a_{p,i}^\dagger), \tag{1b}$$

$$H_{\rm m} = \sum_{j=1}^{2} \nu_j b_j^\dagger b_j, \tag{1c}$$

$$H_{\rm I} = -\sum_{\alpha,j} g_{\alpha j} a_\alpha^\dagger a_\alpha (b_j^\dagger + b_j) \tag{1d}$$

$$H_{\rm d} = -i\Omega(a_c^\dagger - a_c), \tag{1e}$$

where $\delta_\alpha = \omega_\alpha - \omega_l$, the sum over α includes the three photonic modes and g_{cp} accounts for the interaction between the cavity mode and the LSPRs, which depends on the placement of the nanoantennas relative to the optical cavity [38].

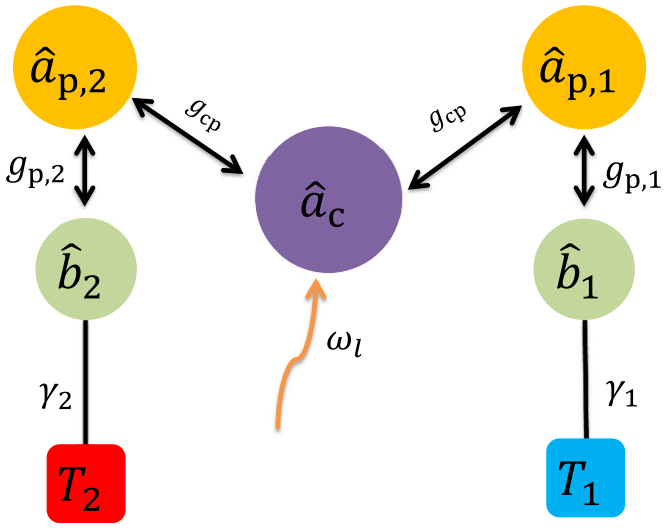

Figure 2. Scheme of the model with all relevant parameters.

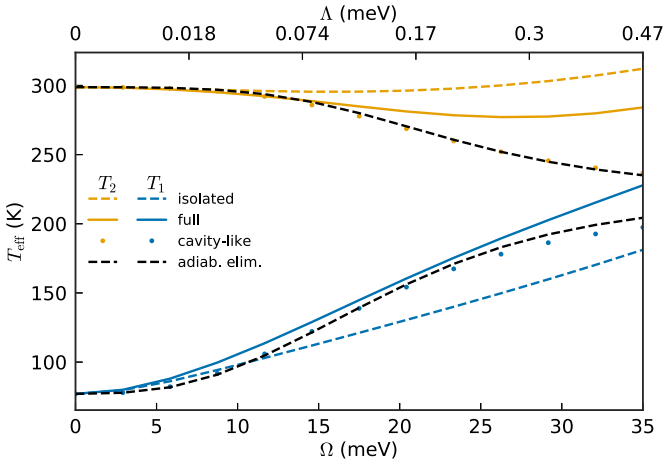

Figure 3. Effective temperature of two identical molecules coupled to heat baths at different temperatures, and indirectly coupled to each other through optomechanical interactions with hybrid cavity modes. The full results (solid lines) are compared to the case of each molecule in isolation (dashed lines), and to the result when only the cavity-like hybrid mode is taken into account (dots) and when that mode is adiabatically eliminated (dashed black lines). Parameters are given in the main text.

Here and in the following, we consider two identical plasmonic cavities placed at equivalent positions sufficiently separated from each other that direct plasmon–plasmon interactions are negligible. The interaction between photonic modes and vibrations, $H_{\rm I}$ is approximated through their optomechanical coupling, which is justified when $\omega_\alpha \gg \nu_j$ [22, 23, 39]. The optomechanical coupling constants are given by $g_{\alpha j} = \frac{\omega_\alpha Q_j^0 R_j}{2\varepsilon\varepsilon_0 V_\alpha}$, where Q_j^0 is the zero point amplitude of vibration j, R_j is its Raman activity, ε is the relative permittivity of the surrounding medium and V_α is the effective mode volume of the photonic mode. Note that the 'bare' photonic mode volume is large ($V \sim \lambda^3 \sim 10^9$ nm^3), so that its direct optomechanical coupling to the molecules is negligible, and that each plasmonic antenna only interacts with its 'own' molecule, $g_{p_1,2} = g_{p_2,1} = 0$.

In addition to the coherent dynamics described by the Hamiltonian, we also model the incoherent dynamics due to the interaction between the different components of the system and their environment. The dynamics of the system density matrix is described within the Lindblad master equation formalism [40]:

$$\frac{\mathrm{d}\rho}{\mathrm{d}t} = -i[H,\rho] + \sum_\alpha L_{a_\alpha}[\rho] + \sum_j L_{b_j}[\rho], \tag{2}$$

with

$$L_{a_\alpha}[\rho] = \kappa_\alpha D_{a_\alpha}[\rho], \tag{3}$$

$$L_{b_j}[\rho] = \gamma_j(\bar{n}_j + 1)D_{b_j}[\rho] + \gamma_j \bar{n}_j D_{b_j^\dagger}[\rho]. \tag{4}$$

Here, κ_α is the decay rate of the photonic mode α, γ_j is the molecular damping rate of molecule j, and $\bar{n}_j = 1/\left[\exp\left(\frac{\nu_j}{k_B T_j}\right) - 1\right]$ is the mean phonon number of molecule j when it is in thermal equilibrium with its associated bath at temperature T_j. Finally, $D_A[\rho]$ is a Lindblad dissipator,

$$D_A[\rho] = A\rho A^\dagger - \frac{1}{2}\{A^\dagger A, \rho\}. \tag{5}$$

In order to quantify the heat transfer between the molecules, we follow the same approach as in our previous paper [24], which we summarize in the following: We first solve for the steady state of the system, $\frac{\mathrm{d}\rho_{\rm ss}}{\mathrm{d}t} = 0$, and then extract an effective temperature for the molecular vibrations,

$$T_j^{\rm eff} = \frac{\nu_j}{k_B \log(1 + 1/n_j)}, \tag{6}$$

based on the average phonon number $n_j = \langle b_j^\dagger b_j \rangle = \mathrm{Tr}(b_j^\dagger b_j \rho_{\rm ss})$. For this effective temperature to correspond to a physical temperature, the population of the energy levels should again follow a thermal distribution. We have checked for all the results presented below that this is indeed the case, i.e. that the steady-state distributions of the phonon populations are well approximated by thermal Boltzmann distributions, and the effective temperatures obtained can thus indeed be interpreted as the steady-state physical temperatures of the respective vibrational modes.

All the numerical results have been obtained using the QuTiP package [41, 42], and plots have been prepared using matplotlib [43, 44]. We note that in contrast to our previous work [24], which used only a single photonic mode, we here treat a relatively big quantum system consisting of five bosonic modes (three photonic and two vibrational) within a density matrix description, such that the numerical size of the density matrix is $5^N \times 5^N$ if N states are used for each mode. The size of the (numerically sparse) Liouvillian superoperator is the square of that number. In order to obtain numerical convergence while keeping the size of the calculations manageable, we use a basis in which the total number of excitations (photons + phonons) is restricted, instead of using a cutoff for

each mode separately. The results presented below use a maximum number of five excitations, which we have checked to give converged results for the parameters used.

3. Results and discussion

We now investigate long-range energy transfer between two molecules, each coupled to a plasmonic nanoantenna with a low-Q resonance, with the two antennas coupled to the same high-Q cavity mode. The model we use is similar to the one proposed by Kamandar Dezfouli, Gordon, and Hughes [38], with the addition of a second plasmonic antenna and molecule. It consists of a photonic crystal supporting a mode with frequency $\omega_c = 1.61$ eV and a high quality factor, $Q_c = 3 \times 10^5$ (i.e. $\kappa_c = 5.4 \times 10^{-2}$ meV), and two identical bowtie nanoantennas separated by a relatively large distance ($\sim\mu$m), with a dipolar LSPR at frequency $\omega_{p,1} = \omega_{p,2} = 2.2$ eV, and relatively low quality factor of $Q_{p,1} = Q_{p,2} = 40$ (i.e. $\kappa_{p,1} = \kappa_{p,2} = 55$ meV). One molecule is placed in the hot spot (i.e. the center) of each nanoantenna. We first treat the case of two identical molecules, with a vibrational mode with angular frequency $\nu_1 = \nu_2 = 40$ meV, and vibrational damping rate of $\gamma_1 = \gamma_2 = 0.1$ meV. Each molecule is coupled to a local heat bath at a different temperature, where here and in the following we set $T_1 = 77$ K, $T_2 = 300$ K. We note that in principle, molecular vibrational frequencies are temperature-dependent due to thermal expansion. For the temperature ranges considered here this effect is typically small (on the order of a 0.5% frequency shift when increasing the temperature from 77 to 300 K) compared to inhomogeneous broadening [45, 46]. The sensitivity of the effects we discuss to such frequency shifts is studied later in the text (figure 5), where we allow the vibrational frequencies of the two molecules to differ. The optomechanical coupling rate for the LSPR modes is taken as $g_p = 75$ meV, corresponding to close-to-resonant Raman transitions [38], while the direct optomechanical coupling to the cavity mode is so small as to have negligible effect (due to the large mode volume). However, the coupling between the cavity mode and each LSPR, with coupling constant $g_{cp} = 200$ meV consistent with values reported in the literature [38], mediates an indirect coupling between the LSPR modes, and thus between the molecules.

We focus on the case where the external laser drives the cavity mode with red detuning, $\omega_l = 1.41$ eV. Figure 3 shows the effective temperature of each molecule as a function of the external laser driving strength Ω. As expected, for $\Omega = 0$, the photonic modes have no influence on the molecules, and each molecular vibration is in equilibrium with its local heat bath. When the laser is turned on, there are two effects on the molecular system. First, the optomechanical coupling for each molecule in isolation can lead to heating and/or cooling of the vibrations through Stokes and anti-Stokes transitions, such that they are driven out of equilibrium with their respective heat baths. This well-known single-molecule effect [39] is shown in dashed lines in figure 3. For the parameters considered here, Stokes processes dominate, resulting in heating for both molecules, significant for the colder molecule (T_1^{eff} increases from 77 to $\approx$170 K), and less pronounced for the hotter molecule (T_2^{eff} increases from 300 to $\approx$315 K). Second, there is an effective molecule-molecule coupling mediated by the photonic modes (through the successive couplings molecule-LSPR-cavity-LSPR-molecule), which enables energy transfer between the molecules, the efficiency of which can be estimated from the effective molecular temperatures (solid lines in figure 3) compared to the single-molecule cases. As seen in figure 3, this can be a significant effect, enabling efficient transfer of energy between the molecules under external pumping of the high-Q cavity mode. For example, for $\Omega = 35$ meV, we obtain $T_1^{\text{eff}} \approx 220$ K, $T_2^{\text{eff}} \approx 280$ K, showing that the hot molecule is efficiently cooled through long-distance heat transfer to the cooler molecule, which is significantly heated in return. The proposed setup could thus indeed be used for externally controlling the heat or energy transfer between molecules that are spatially separated by significant distances. The pumping rate is the main parameter controlling this effect, and increasing it improves the energy exchange, causing the effective temperatures to approach each other.

Additional insight into the long-range heat transfer can be obtained by considering a simplified model where the three photonic modes are diagonalized to obtain hybrid modes (see appendix A for details). In this case, one obtains one high-Q and two lower-Q hybrid modes (one of which is a 'dark' plasmonic mode consisting of the antisymmetric combination of plasmonic antenna modes and does not hybridize with the cavity-like mode). The high-Q mode is dominated by the cavity mode contribution. We thus label it as the 'cavity-like' mode in the following. Considering only the optomechanical interaction with the cavity-like mode (dots in figure 3) reproduces the main effect of optomechanically induced heat transfer, although it underestimates the laser-induced heating, in particular of the hotter molecule. Adiabatically eliminating the cavity-like mode within this single-mode approximation then gives an effective molecule-molecule coupling term $\Lambda(b_1^\dagger b_2 + b_1 b_2^\dagger)$ [24]. The effective temperatures obtained within this approximation (dashed black lines in figure 3, with the corresponding value of Λ shown in the upper axis) reproduce the single-mode results almost perfectly.

We next treat the influence of other parameters on long-distance heat flow between the molecules. We show the effective temperature of the molecules as a function of the coupling rate $\gamma = \gamma_1 = \gamma_2$ between each vibration and its local heat bath in figure 4(a). This rate determines the rate of heat exchange with the local bath, and the temperatures of the vibrational modes thus approach the bath temperatures as γ is increased. For the 'hot' molecule 2, this is enough to make the temperature of the molecule approach its undriven value ($T_2 = 300$ K). While the effect is also very noticeable for the 'cold' molecule, with a decrease in temperature from $\approx$220 to $\approx$110 K as γ is increased from 0.1 to 1 meV, it is not enough to completely counteract the externally induced heat transport. Again, the single-mode approximation only taking into account the cavity-like hybrid mode reproduces the observed trends quite well while underestimating the laser-induced heating of the hotter molecule.

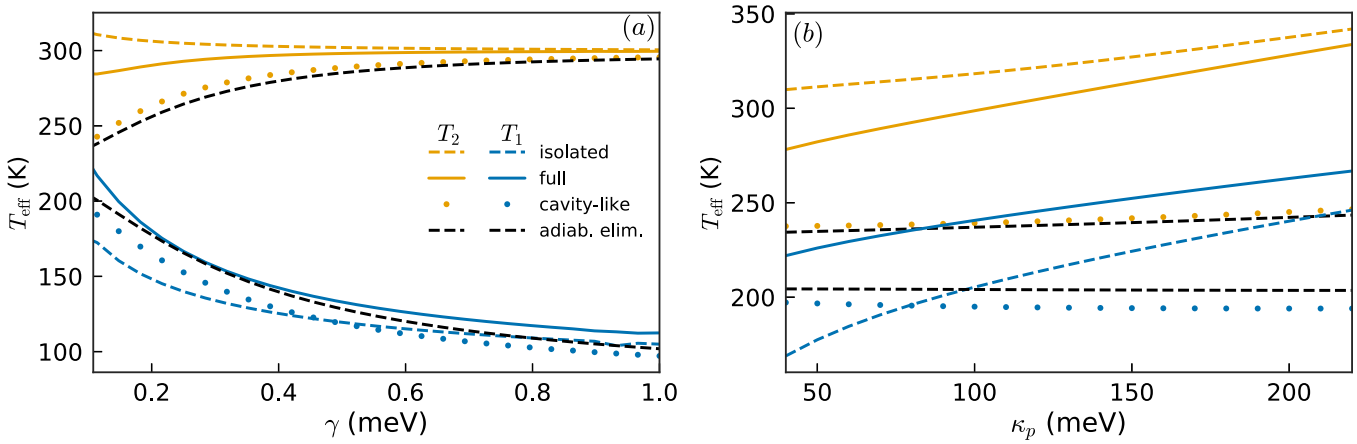

Figure 4. Effective temperature of molecules as a function of (a) molecular damping rate and (b) plasmonic damping rate. The external driving rate is $\Omega = 35$ meV, with all other parameters as in figure 3.

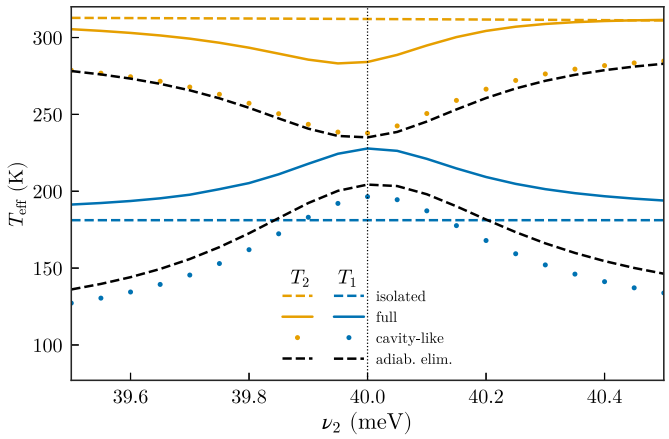

Figure 5. Heat transfer process in the non-symmetric case as a function of the vibrational frequency of the 'hot' molecule 2.

We additionally investigate the effect of the photonic system parameters on the heat transfer effect. In particular, as shown in figure 4(b), an increase in the plasmonic cavity loss $\kappa_p = \kappa_{p,1} = \kappa_{p,2}$ leads to a reduction of heat transfer, while simultaneously inducing more heating on the single-molecule level. As the single-mode approximation that only takes into account the high-Q cavity-like mode underestimates the plasmon-induced heating, it is not capable of reproducing this trend accurately, and the effective temperatures within this approximation are approximately constant as a function of κ_p, see the dots in figure 4(b). The effect seen here shows that it is desirable to use plasmonic nanoantennas of the highest quality possible to minimize direct optomechanical heating while simultaneously reaching large effective optomechanical coupling strengths. Similarly, we find that improving the quality factor of the delocalized cavity mode (i.e. decreasing its loss rate) also leads to improved heat transfer (not shown).

We now treat the non-symmetric case where the vibrational frequencies of the two molecules are not identical (while keeping all other parameters fixed for simplicity), i.e. we explore whether it is possible to enable heat transfer between molecules even if their vibrational frequencies are not equal. In addition to the case of two different molecules with similar vibrational transitions, such differences can be due to inhomogeneous broadening, i.e. energy shifts for each individual molecule, as well as due to the temperature dependence of the vibrational frequencies [45, 46]. In figure 5, we plot the effective vibrational temperatures of the two molecules when the vibrational frequency ν_2 of the 'hot' molecule is changed, with ν_1 fixed at 40 meV and all other parameters as in figure 3.We find relatively efficient heat transfer only when the two vibrations are close to resonance ($\nu_1 \approx \nu_2$). These results are consistent with the case where two molecules are coupled to the *same* plasmonic nanocavity mode [24], and imply that a single-vibrational-mode approximation is justified.

To gain a better understanding of this effect, we next analyze the power spectral density (PSD) of the involved modes, which measures their oscillation spectrum as a function of frequency [47]. The PSD for a mode with annihilation operator A is given by the Fourier transform of the correlation spectrum of the operator in the steady state,

$$S_A(\omega) = \int e^{-i\omega t} \left\langle A^\dagger(t) A(0) \right\rangle_{\rm ss} {\rm d}\omega. \tag{7}$$

The PSD for the symmetric case of identical molecular vibrations is shown in figure 6(a). For the photonic mode basis, we here use the hybrid photonic modes obtained after diagonalizing the coupled cavity and LSPR modes. This figure shows that the cavity-like hybrid mode (black dashed line) is the principal photonic mode involved in the dynamics, with a modulation imprinted on it at frequencies close to the vibrational ones. As discussed previously, this mode mediates the effective long-range molecule–molecule coupling. In the current regime, the effective linewidth of the PSD of the cavity-like mode is *not* determined by its loss rate ($\kappa_- \approx 8$ meV), but much closer to the molecular vibrational linewidth. When the two molecular vibrations are detuned from each other, shown in figure 6(b) for vibrational frequencies $\nu_1 = 40$ meV and $\nu_2 = 37$ meV, each molecule only oscillates at its native frequency, and the cavity-like mode has two essentially independent peaks at ν_1

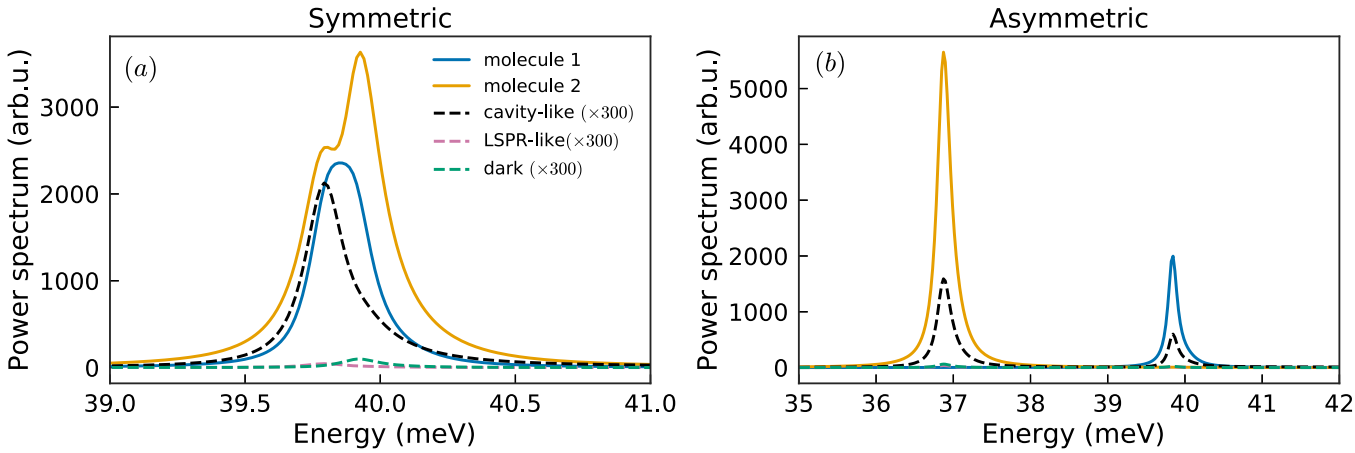

Figure 6. (a) Power spectral density in symmetric system for hot molecule (red solid line), cold molecule (blue solid line) and the PC mode (orange dashed). (b) The PSD for non-symmetric system when $\nu_1 = 50$ meV, $\nu_2 = 47$ meV.

and ν_2. The off-resonant fluctuations induced on the cavity-like mode by the two vibrational modes then prevent effective long-range energy transfer between them.

4. Summary and conclusions

To summarize, we have theoretically and numerically investigated the optomechanical heat transfer mechanism between two spatially separated molecules at different local temperatures placed in a hybrid plasmonic-photonic nanoresonator. The hybrid cavity considered consists of two plasmonic nanoantennas supporting LSPR modes that are both coupled to the same high-quality cavity mode (such as supported by a photonic crystal cavity or a Fabry–Perot cavity with highly reflective mirrors). The cavity mode is driven by an external red-detuned laser. We have shown that in such a hybrid setup, the cavity-like mode, which itself has negligible optomechanical coupling to the molecular vibrations, can behave like a mediator that provides an effective molecule–molecule coupling over large distances of the order of several free-space wavelengths, while the strongly sub-wavelength plasmonic modes provide the required large optomechanical coupling strengths. The hybrid setup considered can thus induce long-range heat transfer between molecules. Additionally, the heat transfer is fully controlled by an external driving laser, and can thus be dynamically turned off or on. Furthermore, we have found that this mechanism only occurs for close-to-resonant vibrational modes, which can be understood by considering the molecule-induced oscillation of the hybrid cavity modes through their power spectral density.

Acknowledgments

This work has been funded by the European Research Council through grant ERC-2016-StG-714870 and by the Spanish Ministry for Science, Innovation, and Universities—Agencia Estatal de Investigación through Grant Nos. RTI2018-099737-B-I00, PCI2018-093145 (through the QuantERA program of the European Commission), and MDM-2014-0377 (through the María de Maeztu program for Units of Excellence in R&D), as well as through a Ramón y Cajal grant (J F) and support from the Iranian Ministry of Science, Research and Technology (SMA).

Appendix A Hybrid modes

We here discuss the properties of the hybrid modes obtained by diagonalizing the 'photonic' subsystem consisting of the cavity mode and two localized surface plasmon resonances. The photonic Hamiltonian can be written as $H_{\rm ph} = \vec{A}^\dagger \boldsymbol{\mathcal{H}} \vec{A}$, where $\vec{A} = (a_c, a_{p,1}, a_{p,2})^T$ collects the photonic annihilation operators and the matrix $\mathcal{H}$ is

$$\boldsymbol{\mathcal{H}} = \begin{pmatrix} \delta_p & 0 & g_{cp} \\ 0 & \delta_p & g_{cp} \\ g_{cp} & g_{cp} & \delta_c \end{pmatrix}. \tag{A1}$$

Diagonalization of $\boldsymbol{\mathcal{H}}$ gives the hybrid mode energies

$$\delta_\pm = \frac{\delta_p + \delta_c}{2} \pm \frac{1}{2}\sqrt{(\delta_p - \delta_c)^2 + 8g_{cp}^2}, \tag{A2}$$

$$\delta_D = \delta_p, \tag{A3}$$

and annihilation operators

$$a_- = \cos\theta a_c + \frac{\sin\theta}{\sqrt{2}}(a_{p,1} + a_{p,2}), \tag{A4}$$

$$a_+ = -\sin\theta a_c + \frac{\cos\theta}{\sqrt{2}}(a_{p,1} + a_{p,2}), \tag{A5}$$

$$a_D = \frac{1}{\sqrt{2}}(a_{p,1} - a_{p,2}), \tag{A6}$$

where $\tan 2\theta = \sqrt{8}g_{cp}/(\delta_p - \delta_c)$. If the coupling g_{cp} is not too large compared to the detuning $\delta_p - \delta_c$, the hybrid modes are a 'small' rotation of the original basis and can be identified as a cavity-like hybrid mode (a_-), an LSPR-like hybrid mode (a_+), and an LSPR dark mode a_D that has no cavity contribution. The original operators can be represented in the new basis as

$$a_c = \cos\theta a_- - \sin\theta a_+, \tag{A7}$$

$$a_{p,1} = \frac{1}{\sqrt{2}}(\sin\theta a_- + \cos\theta a_+ + a_D), \tag{A8}$$

$$a_{p,2} = \frac{1}{\sqrt{2}}(\sin\theta a_- + \cos\theta a_+ - a_D). \tag{A9}$$

The changed parts of the Hamiltonian in the new hybrid basis are given by

$$H_{\rm ph} = \sum_\beta \delta_\beta a_\beta^\dagger a_\beta, \tag{A10a}$$

$$H_{\rm I} = -\sum_{\beta,j} g_\beta a_\beta^\dagger a_\beta (b_j^\dagger + b_j) - \sum_{\beta'>\beta,j} g_{\beta'\beta}(a_\beta^\dagger a_{\beta'} + a_\beta a_{\beta'}^\dagger)(b_j^\dagger + b_j), \tag{A10b}$$

$$H_{\rm d} = i\Omega\cos\theta(a_-^\dagger - a_-) - i\Omega\sin\theta(a_+^\dagger - a_+), \tag{A10c}$$

where $\beta \in -,+,D$ runs over the hybrid modes, and

$$g_- = \sin^2\theta\frac{g_p}{2}, \qquad g_{+-} = \sin\theta\cos\theta\frac{g_p}{2}, \tag{A11a}$$

$$g_+ = \cos^2\theta\frac{g_p}{2}, \qquad g_{D-} = \sin\theta\frac{g_p}{2}, \tag{A11b}$$

$$g_D = \frac{g_p}{2}, \qquad g_{D+} = \cos\theta\frac{g_p}{2}. \tag{A11c}$$

The dynamics is then described by the master equation

$$\frac{{\rm d}\rho}{{\rm d}t} = -i[H,\rho] + \sum_\beta L_{a_\beta}[\rho] + \sum_j L_{b_j}[\rho] + \bar{L}_\pm[\rho], \tag{A12}$$

where

$$L_{a_\beta}[\rho] = \kappa_\beta D_{a_\beta}[\rho], \tag{A13a}$$

$$\bar{L}_\pm[\rho] = \kappa_\pm(D_{a_+,a_-}[\rho] + D_{a_-,a_+}[\rho]), \tag{A13b}$$

where $D_{a,b}[\rho] = a\rho b^\dagger - \frac{1}{2}\{b^\dagger a, \rho\}$ and

$$\kappa_D = \kappa_p, \tag{A14a}$$

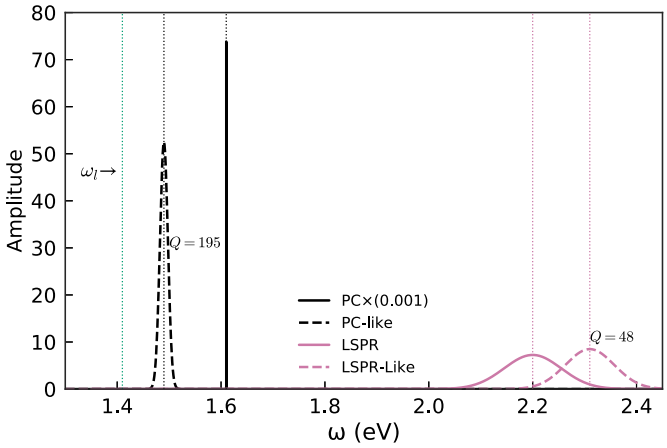

Figure A1. Comparison between the original (solid lines) and hybrid (dashed lines) modes of the system. Each mode is represented by a Lorentzian at frequency ω_β with linewidth κ_β and amplitude g_β. The driving laser frequency ω_l is indicated by a thin blue-green dotted line.

$$\kappa_- = \cos^2\theta\kappa_c + \sin^2\theta\kappa_p, \tag{A14b}$$

$$\kappa_+ = \cos^2\theta\kappa_p + \sin^2\theta\kappa_c, \tag{A14c}$$

$$\kappa_\pm = (\kappa_p - \kappa_c)\sin\theta\cos\theta. \tag{A14d}$$

The properties of the hybrid modes are shown schematically in figure A1, where each mode is represented by a Lorentzian at frequency $\omega_\beta = \delta_\beta + \omega_l$, with linewidth κ_β and amplitude g_β. The driving laser is indicates as a dotted blue-green line at $\omega_l = 1.41$ eV. For the parameters considered, the cavity-like mode a_- thus clearly gives the most significant contribution since it is close to resonance with the external laser and has a strong optomechanical interaction. The simplified effective Hamiltonian obtained by only taking into account the hybrid cavity-like mode is given by

$$H_{\rm hc} \approx \delta_- a_-^\dagger a_- + \nu_1 b_1^\dagger b_1 + \nu_2 b_2^\dagger b_2 + i\Omega\cos\theta(a_-^\dagger - a_-) - g_- a_-^\dagger a_-(b_1^\dagger + b_1 + b_2^\dagger + b_2). \tag{A15}$$

The results obtained with this Hamiltonian are shown in the main text as the 'cavity-like' approximation.

ORCID iDs

S Mahmoud Ashrafi https://orcid.org/0000-0002-8444-4391
R Malekfar https://orcid.org/0000-0001-5529-5983
Johannes Feist https://orcid.org/0000-0002-7972-0646

References

[1] Nagali E, Sciarrino F, De Martini F, Marrucci L, Piccirillo B, Karimi E and Santamato E 2009 Quantum information transfer from spin to orbital angular momentum of photons *Phys. Rev. Lett.* **103** 013601

[2] Northup T E and Blatt R 2014 Quantum information transfer using photons *Nat. Photonics* **8** 356

[3] Nalbach P, Eckel J and Thorwart M 2010 Quantum coherent biomolecular energy transfer with spatially correlated fluctuations *New J. Phys.* **12** 065043

[4] Dubi Y and Ventra M Di 2011 Colloquium: heat flow and thermoelectricity in atomic and molecular junctions *Rev. Mod. Phys.* **83** 131

[5] Katz G and Kosloff R 2016 Quantum thermodynamics in strong coupling: heat transport and refrigeration *Entropy* **18** 186

[6] Lee H, Cheng Y-C and Fleming G R 2007 Coherence dynamics in photosynthesis: protein protection of excitonic coherence *Science* **316** 1462

[7] Scholes G D, Fleming G R, Olaya-Castro A and Grondelle R van 2011 Lessons from nature about solar light harvesting *Nat. Chem.* **3** 763

[8] High A A, Novitskaya E E, Butov L V, Hanson M and Gossard A C 2008 Control of exciton fluxes in an excitonic integrated circuit *Science* **321** 229

[9] Matthew Menke S, Luhman W A and Holmes R J 2012 Tailored exciton diffusion in organic photovoltaic cells for enhanced power conversion efficiency *Nat. Mater.* **12** 152

[10] Gerry C and Knight P 2004 *Introductory Quantum Optics* (Cambridge: Cambridge University Press)

[11] Messina R, Antezza M and Ben-Abdallah P 2012 Three-body amplification of photon heat tunneling *Phys. Rev. Lett.* **109** 244302

[12] Feist J and Garcia-Vidal F J 2015 Extraordinary exciton conductance induced by strong coupling *Phys. Rev. Lett.* **114** 196402

[13] Schachenmayer J, Genes C, Tignone E and Pupillo G 2015 Cavity-enhanced transport of excitons *Phys. Rev. Lett.* **114** 196403

[14] Kim M-K, Sim H, Yoon S J, Gong S-H, Ahn C W, Cho Y-H and Lee Y-H 2015 Squeezing photons into a point-like space *Nano Lett.* **15** 4102

[15] Chikkaraddy R *et al* 2016 Single-molecule strong coupling at room temperature in plasmonic nanocavities *Nature* **535** 127

[16] Ojambati O S, Chikkaraddy R, Deacon W D, Horton M, Kos D, Turek V A, Keyser U F and Baumberg J J 2019 Quantum electrodynamics at room temperature coupling a single vibrating molecule with a plasmonic nanocavity *Nat. Commun.* **10** 1049

[17] Fernández-Domínguez A I, García-Vidal F J and Martín-Moreno L 2017 Unrelenting plasmons *Nat. Photonics* **11** 8

[18] Hoang T B, Akselrod G M and Mikkelsen M H 2016 Ultrafast room-temperature single photon emission from quantum dots coupled to plasmonic nanocavities *Nano Lett.* **16** 270

[19] Straubel J, Sarniak R, Rockstuhl C and Słowik K 2017 Entangled light from bimodal optical nanoantennas *Phys. Rev.* B **95** 085421

[20] Kneipp K, Moskovits M and Kneipp H 2006 *Surface-Enhanced Raman Scattering: Physics and Applications (Topics in Applied Physics)* 1st edn (Berlin: Springer)

[21] Schlücker S 2014 Surface-enhanced Raman spectroscopy: concepts and chemical applications *Angew. Chem. Int. Ed.* **53** 4756

[22] Roelli P, Galland C, Piro N and Kippenberg T J 2016 Molecular cavity optomechanics as a theory of plasmon-enhanced Raman scattering *Nat. Nanotechnol.* **11** 164

[23] Schmidt M K, Esteban R, González-Tudela A, Giedke G and Aizpurua J 2016 Quantum mechanical description of Raman scattering from molecules in plasmonic cavities *ACS Nano* **10** 6291

[24] Mahmoud Ashrafi S, Malekfar R, Bahrampour A R and Feist J 2019 Optomechanical heat transfer between molecules in a nanoplasmonic cavity *Phys. Rev.* A **100** 013826

[25] Xiao Y-F, Liu Y-C, Bei-Bei Li, Chen Y-L, Yan Li and Gong Q 2012 Strongly enhanced light-matter interaction in a hybrid photonic-plasmonic resonator *Phys. Rev.* A **85** 031805

[26] Conteduca D, Reardon C, Scullion M G, Dell'Olio F, Armenise M N, Krauss T F and Ciminelli C 2017 Ultra-high Q/V hybrid cavity for strong light-matter interaction *APL Photonics* **2** 086101

[27] Gurlek B, Sandoghdar V and Martín-Cano D 2018 Manipulation of quenching in nanoantenna–emitter systems enabled by external detuned cavities: a path to enhance strong-coupling *ACS Photonics* **5** 456

[28] Mossayebi M, Wright A J, Parini A, Somekh M G, Bellanca G and Larkins E C 2016 Investigating the use of a hybrid plasmonic–photonic nanoresonator for optical trapping using finite-difference time-domain method *Opt. Quant. Electron.* **48** 275

[29] Peyskens Féric, Dhakal A, Van Dorpe P, Le Thomas N and Baets R 2016 Surface enhanced Raman spectroscopy using a single mode nanophotonic-plasmonic platform *ACS Photonics* **3** 102

[30] De Angelis F, Patrini M, Das G, Maksymov I, Galli M, Businaro L, Andreani L C and Fabrizio E Di 2008 A hybrid plasmonic-photonic nanodevice for label-free detection of a few molecules *Nano Lett.* **8** 2321

[31] Dantham V R, Holler S, Barbre C, Keng D, Kolchenko V and Arnold S 2013 Label-free detection of single protein using a nanoplasmonic-photonic hybrid microcavity *Nano Lett.* **13** 3347

[32] Conteduca D, Dell'Olio F, Innone F, Ciminelli C and Armenise M N 2016 Rigorous design of an ultra-high Q/V photonic/plasmonic cavity to be used in biosensing applications *Opt. Laser Technol.* **77** 151

[33] Xavier J, Vincent S, Meder F and Vollmer F 2018 Advances in optoplasmonic sensors–combining optical nano/microcavities and photonic crystals with plasmonic nanostructures and nanoparticles *Nanophotonics* **7** 1

[34] Hu Y-W, Li B-B, Liu Y-X, Xiao Y-F and Gong Q 2013 Hybrid photonic–plasmonic mode for refractometer and nanoparticle trapping *Opt. Commun.* **291** 380

[35] Hughes S, Richter M and Knorr A 2018 Quantized pseudomodes for plasmonic cavity QED *Opt. Lett.* **43** 1834

[36] Franke S, Hughes S, Dezfouli M K, Trøst Kristensen P, Busch K, Knorr A and Richter M 2019 Quantization of quasinormal modes for open cavities and plasmonic cavity quantum electrodynamics *Phys. Rev. Lett.* **122** 213901

[37] Medina I, García-Vidal F J, Fernández-Domínguez A I and J F 2020 Few-mode field quantization of arbitrary electromagnetic spectral densities (arxiv.org:2008.00349)

[38] Dezfouli M K, Gordon R and Hughes S 2019 Molecular optomechanics in the anharmonic cavity-QED regime using hybrid metal–dielectric cavity modes *ACS Photonics* **6** 1400

[39] Schmidt M K, Esteban R, Benz F, Baumberg J J and Aizpurua J 2017 Linking classical and molecular optomechanics descriptions of SERS *Faraday Discuss.* **205** 31

[40] Breuer H-P and Petruccione F 2007 *The Theory of Open Quantum Systems* (Oxford: Oxford University Press)

[41] Johansson J R, Nation P D and Nori F 2012 QuTiP: an open-source python framework for the dynamics of open quantum systems *Comput. Phys. Commun.* **183** 1760

[42] Johansson J R, Nation P D and Nori F 2013 QuTiP 2: a python framework for the dynamics of open quantum systems *Comput. Phys. Commun.* **184** 1234

[43] Hunter J D 2007 Matplotlib: a 2D graphics environment *Comput. Sci. Eng.* **9** 90

[44] Caswell T A *et al* 2020 Matplotlib v3.2.1 *Zenodo* (https://doi.org/10.5281/zenodo.3714460)
[45] Artur C, Le Ru E C and Etchegoin P G 2011 Temperature dependence of the homogeneous broadening of resonant Raman peaks measured by single-molecule surface-enhanced Raman spectroscopy *J. Phys. Chem. Lett.* **2** 3002
[46] Park K-D, Muller E A, Kravtsov V, Sass P M, Dreyer J, Atkin J M and Raschke M B 2016 Variable-temperature tip-enhanced Raman spectroscopy of single-molecule fluctuations and dynamics *Nano Lett.* **16** 479
[47] Gardiner C W and Zoller P 2004 *Quantum Noise: A Handbook of Markovian and Non-Markovian Quantum Stochastic Methods with Applications to Quantum Optics* (Berlin: Springer)